Shell filling of artificial atoms within density-functional theory

In-Ho Lee
Beckman Institute for Advanced Science and Technology, University of Illinois at Urbana-Champaign, Urbana, Illinois 61801

Vivek Rao
Department of Physics and Materials Research Laboratory, University of Illinois at Urbana-Champaign, Urbana, Illinois 61801

Richard M. Martin
Beckman Institute for Advanced Science and Technology, University of Illinois at Urbana-Champaign, Urbana, Illinois 61801 and Department of Physics and Materials Research Laboratory, University of Illinois at Urbana-Champaign, Urbana, Illinois 61801

Jean-Pierre Leburton
Beckman Institute for Advanced Science and Technology, University of Illinois at Urbana-Champaign, Urbana, Illinois 61801
(Received 30 September 1997)

The electronic structures of three-dimensional quantum dots described by parabolic and nonparabolic confinements are calculated using spin-density-functional theory. For representative cases we determined the electron-number-dependent capacitive energy, the energy required to add an additional electron to a quantum dot, by self-consistent solution of the equations using a finite difference method with preconditioned conjugate gradient minimization. Shell-filling and spin configuration effects are identified, as found in electronic structure of the atoms. The peak positions of the capacitive energy at the number of electrons $N=2$, 6, and 12 for the cylindrical symmetric quantum dot are in good agreement with experimental data. [S0163-1829(98)04811-5]

I. INTRODUCTION

With the development of the x-ray lithography, etching, and deposition techniques in semiconductor technology, it is possible to confine electrons in a small region known as a quantum dot.[1] The electronic structure of these confined electrons is very important and interesting in the area of basic and applied physics. The confining potential of the order of a few meV can be chosen experimentally. Many-body effects due to the electron-electron interactions show a broad range of electronic structures similar to those of the real atoms. The number of electrons in a quantum dot, denoted N, which can also be controlled experimentally, affects many physical properties of the quantum dot. The dependence of the chemical potential on N was directly measured through single-electron spectroscopy.[2–4] By changing the quantum dot size and the number of electrons, far-infrared absorption,[5–7] capacitance spectroscopy,[8] and conductance measurements[2,3] determine the tunneling conductance and capacitance resulting from the competition of quantum confinements and Coulomb interactions.

Electron-electron interactions in low-dimensional systems are calculated through various theoretical approaches.[9–21] The capacitance of the quantum dot is an interesting concept related to the single-electron tunneling and the Coulomb blockade phenomenon. Recently, Tarucha *et al.* probed the electronic states of a few-electron quantum dot through single-electron tunneling spectroscopy.[4] They also measured the effects of spin configuration and confirmed Hund's rule favoring the filling of parallel spins by applying tunable magnetic fields to the quantum dots. Furthermore, Macucci *et al.* have calculated the shell-filling behavior of two-dimensional cylindrical quantum dots within the framework of density-functional theory.[20,21] Fujito, Natori, and Yasunaga studied the many-electron ground state in parabolic quantum dots using the unrestricted Hartree-Fock method and found capacitance oscillations as a function of the electron number caused by the shell structure.[19]

We have calculated the electronic structure of three-dimensional anisotropic quantum dots through the finite difference method with preconditioned conjugate gradient relaxation based on the density-functional theory. The capacitive energy of up to thirteen electrons is obtained through a self-consistent total-energy calculation for model three-dimensional quantum dots. Since the exclusion principle prevents two same-spin electrons from having the same spatial wave function, the spin configuration in the quantum dots plays an important role, as it does in atomic physics. The explicit electron-spin interactions are taken into account via spin-density-functional theory, which properly describes the spin effects of atomic systems. We studied the effects of symmetry and nonparabolicity in the confinement potentials on the electronic structure of the quantum dot. We also compared the calculated results of the spin-polarized calculations with unpolarized total energy calculation, different exchange-correlation energy per particle, and the Hartree approximations.

The outline of this paper is as follows. In Sec. II, we present our theoretical method. The calculational results and discussion are shown in Sec. III. A brief summary is given in Sec. IV.

II. THEORETICAL METHODS

In the present calculations we assumed the quantum dot is well isolated so that the interaction between the dot and leads

or other conductors in real quantum dots is negligible; in doing so we have not included the effects of gates and adjacent conducting materials. Within the effective mass approximation and density-functional theory, one can write the simple effective quantum dot Hamiltonian,

$$H=-\tfrac{1}{2}\vec{\nabla}^2+\tfrac{1}{2}\omega_x^2x^2+\tfrac{1}{2}\omega_y^2y^2+\tfrac{1}{2}\omega_z^2z^2+V_H(\vec{r})+V_{xc}(\vec{r}), \tag{1}$$

including the external potentials described by ω_x, ω_y, and ω_z of the anisotropic parabolic three-dimensional potential, Hartree $V_H(\vec{r})$, and exchange correlation $V_{\mathrm{xc}}(\vec{r})$ as shown in Eq. (1). Rescaled atomic units are used throughout, with energy in units of 2 Ry$^*=m^*e^4/\hbar^2\varepsilon^2$ and lengths in units of the effective Bohr radius $a_B^*=\hbar^2\varepsilon/m^*e^2$. The effective mass and the dielectric constant are denoted by m^* and ε, respectively. We used the finite difference formula for the Laplacian operator in the Hamiltonian,[22,23] with a seven-point stencil in each direction, and iteratively diagonalized the Hamiltonian in three-dimensional Cartesian coordinates with uniform grids.

Spin-polarized Kohn-Sham equations[24,25] were solved self-consistently to calculate the total energy of the quantum dots. The Hartree potential and energy due to the electrons in the quantum dot were obtained by solving the Poisson equation using the preconditioned conjugate gradient method. The boundary values of Hartree potential were evaluated using a multipole expansion of the potential of the charge-density distribution. This method is very efficient compared to the direct integration of the potential at the surfaces. The multipole expansion is accurate if the charge distribution is well localized within the computational box. The relaxation vectors at the boundary are set to zero for the Dirichlet boundary conditions. We have used the generalized-gradient approximation (GGA) for the exchange-correlation energy and potential to incorporate the effects of the gradient correction of the local-density approximation (LDA). We used the simplified version of the recent GGA functional by Perdew, Burke, and Ernzerhof,[26] which satisfies many exact properties of density-functional theory such as the accurate description of the linear response of the uniform electron gas and proper uniform scaling. The GGA expression for the exchange-correlation energy per particle gives better descriptions of the total energy and the ionization energy for the atoms compared to the LDA.[26] For the LDA calculations, we used the exchange-correlation energy and potential based on the quantum Monte Carlo simulation data of the uniform electron gas.[27]

In the present iterative relaxation procedures for solving the Poisson and Kohn-Sham equations the explicit evaluation and the storage of the Hamiltonian matrix can be avoided. The matrix-vector multiplication is replaced by the finite difference operation on the vector represented in three-dimensional space, resulting in a simple linear combination of the adjacent components of the vector. This procedure leads to a great saving of computational resources. We used the preconditioned conjugate gradient type relaxations with the constraint of orthonormalization conditions between the states to obtain the occupied states and a few lowest unoccupied states (eigenvalues and eigenvectors) of the large size of the Hamiltonian matrix.[28] We also included the subspace diagonalization after band by band minimization of the Kohn-Sham orbitals.[29]

In the conjugate gradient algorithm the residuals and the searching directions are orthogonal for each different relaxation step and the relaxations guarantee convergence if the matrix is symmetric positive-definite. The uniform grids give a symmetric matrix representation of the nonlocal Laplacian operator in Kohn-Sham and Poisson equations. Roughly speaking, the preconditioning of the relaxation vector can be considered as a procedure of smoothing of the relaxation vectors in real space. To reduce the number of conjugate gradient relaxation steps, we used the two different preconditioning operators found in the literature. For solving the Poisson equation, we have used the following form of preconditioning operator $\hat{P}$ of fifth order proposed by Hoshi, Arai, and Fujiwara,[30] which filters out the high-frequency components of the relaxation vector $u(\vec{r})$,

$$(\hat{P}u)(\vec{r})=\frac{1}{2}\left\{u(\vec{r})+\sum_{\Delta\vec{r}=h(\pm1,\pm1,\pm1)}\frac{u(\vec{r}+\Delta\vec{r})}{6}\right\}. \tag{2}$$

We also used the preconditioning operator proposed by Seitsonen, Puska, and Nieminen[31] for the iterative diagonalizations. We have found that the preconditioning of Hoshi, Arai, and Fujiwara does not work properly for the relaxation of especially slow-varying (or low kinetic energy) states, because the preconditioning of Hoshi, Arai, and Fujiwara is short ranged and has no dependence on the kinetic energy of the current trial wave function.

To accelerate the self-consistency calculations we used the Pulay-type charge[32] density-mixing scheme for each up- and down-spin density during the iterations. This relaxation minimizes the difference between input and output charge densities in the self-consistent loop with the constraint of charge conservation. The optimal input charge density is expressed as a linear combination of a few previous input densities. In our calculations we have taken the effective kinetic energy cutoff $(\pi/h)^2$ Ry$^*\approx110$ Ry* related to the uniform grid spacing h in a_B^* as found in usual plane-wave basis set formulation. We also made convergence tests on physical observables with respect to the grid spacing h. The typical number of grid points used for the single-particle wave function for the large quantum dot in the present calculation is about 138 000.

The total energy of the model quantum dot in density-functional theory can be expressed as follows:

$$\begin{aligned}E=&\sum_{\epsilon_i^{\uparrow}<\epsilon_F}\epsilon_i^{\uparrow}-\int\{\tilde{V}_H(\vec{r})+\tilde{V}_{\mathrm{xc}}^{\uparrow}(\vec{r})\}\rho^{\uparrow}(\vec{r})d^3r\\&+\sum_{\epsilon_i^{\downarrow}<\epsilon_F}\epsilon_i^{\downarrow}-\int\{\tilde{V}_H(\vec{r})+\tilde{V}_{\mathrm{xc}}^{\downarrow}(\vec{r})\}\rho^{\downarrow}(\vec{r})d^3r\\&+\frac{1}{2}\int V_H(\vec{r})[\rho^{\uparrow}(\vec{r})+\rho^{\downarrow}(\vec{r})]d^3r+E_{\mathrm{xc}}[\rho^{\uparrow}(\vec{r}),\rho^{\downarrow}(\vec{r})],\end{aligned} \tag{3}$$

where the summations over the single spin eigenenergy ($\epsilon_i^{\uparrow}$ and $\epsilon_i^{\downarrow}$) are carried on for all states below the Fermi level

ϵ_F. The electron densities $\rho^{\uparrow}(\vec{r})$ and $\rho^{\downarrow}(\vec{r})$ are defined as the squared summation of the occupied Kohn-Sham orbitals, and $E_{\rm xc}[\rho^{\uparrow}(\vec{r}),\rho^{\downarrow}(\vec{r})]$ is the total exchange-correlation energy. $\widetilde{V}_H(\vec{r})$, $\widetilde{V}^{\uparrow}_{\rm xc}(\vec{r})$, and $\widetilde{V}^{\downarrow}_{\rm xc}(\vec{r})$ represent the *input* electronic potentials for the Hartree and exchange-correlation (up and down spin) contributions at each iteration within the self-consistent calculations. All other quantities, i.e., $V_H(\vec{r})$, $\rho^{\uparrow}(\vec{r})$, $\rho^{\downarrow}(\vec{r})$, and $E_{\rm xc}[\rho^{\uparrow}(\vec{r}),\rho^{\downarrow}(\vec{r})]$ are evaluated using the *output* charge densities of the self-consistent iterations. Hence the two quantities $\widetilde{V}_H(\vec{r})+\widetilde{V}^{\uparrow}_{\rm xc}(\vec{r})$ and $\widetilde{V}_H(\vec{r})+\widetilde{V}^{\downarrow}_{\rm xc}(\vec{r})$ are very close to the corresponding Hartree-exchange-correlation potentials given by output charge densities when self-consistency is established. Thus, the first four terms in Eq. (3) decomposed into up- and down-spin state contributions, represent the sum of the total kinetic and external potential energy.

To calculate the capacitive energy of a quantum dot, which indicates the variation of the dot total energy as a function of the number of electrons, we followed the formulation of Iafrate *et al.*[18] for the specific dielectric constant and electron effective mass of the semiconductor material system. The chemical potential $\mu(N)$ for N electrons can be defined by the total energy difference between the number of N and the number of $N-1$ electrons as follows:

$$\mu(N)=E(N)-E(N-1). \tag{4}$$

The chemical potential is the energy required to add one electron to the system with $N-1$ electrons. From the chemical potential, one can derive the capacitance $C(N)$ of the quantum dots, the energy required to add charge e,[1,18]

$$C(N)=\frac{e^2}{\mu(N+1)-\mu(N)}. \tag{5}$$

The capacitive energy $e^2/C(N)$ is easily reduced to the simple relation between[1,18] the ionization potential $I(N)$ and the electron affinity $A(N)$ of an N particle system as shown in Eq. (6):

$$\begin{aligned}\frac{e^2}{C(N)}&=\mu(N+1)-\mu(N)\\&=\{E(N+1)-E(N)\}-\{E(N)-E(N-1)\}\\&=\{E(N-1)-E(N)\}-\{E(N)-E(N+1)\}\\&=I(N)-A(N).\end{aligned} \tag{6}$$

Furthermore, in the density-functional theory the capacitive energy is also approximated by the gap defined by the eigenvalue difference between the lowest unoccupied $\epsilon^{\rm LU}(N)$ and the highest occupied $\epsilon^{\rm HO}(N)$ states for an N electron system. The capacitive energy satisfies the relation of

$$I(N)-A(N)\sim\epsilon^{\rm LU}(N)-\epsilon^{\rm HO}(N). \tag{7}$$

III. RESULTS AND DISCUSSION

A. Cylindrically symmetric confinement ($\omega_x=\omega_y$)

We calculated the electronic structure of GaAs quantum dots by using the dielectric constant of $\varepsilon=12.9$ and effective mass of $m^*=0.067m_e$. The corresponding energy and length scales are 2 Ry*=10.96 meV and $a_B^*=101.88$ Å, respectively. We first considered a system with isotropic confinement in the x-y plane to investigate the effects of the cylindrical symmetry. Electrons are confined in the z direction by the relatively strong harmonic potential. We choose the ω_z=45 meV to approximate the thickness of the quasi-two-dimensional electron gas in experiments. From the choice of ω_z=45 meV, we can calculate the characteristic length of harmonic oscillator $l_c=\omega_z^{-1/2}$ and assign the thickness of two-dimensional model electron gas by $2\times l_c\approx 10.1$ nm. We also treat the cases of $\omega_x\neq\omega_y$ and nonparabolic confinement in the next subsections. In Fig. 1 we plot the total energy $E(N)$, chemical potential $\mu(N)$, and the capacitive energy $\mu(N+1)-\mu(N)$ as a function of the number of electrons in the quantum dot. The circles, boxes, and triangles represent the confinement potential parameters $\omega_x=\omega_y$ (in units of meV) 20, 10, and 4, respectively. Here, we also show the spin polarization, $N^{\uparrow}-N^{\downarrow}/N^{\uparrow}+N^{\downarrow}$, where $N^{\uparrow}$ and $N^{\downarrow}$ are integers that denote the number of electrons with spin up and spin down. The ground states are determined by self-consistent total energy calculations incorporating spin-polarization effects. The capacitive energy $\mu(N+1)-\mu(N)$ of up to thirteen electrons is obtained through

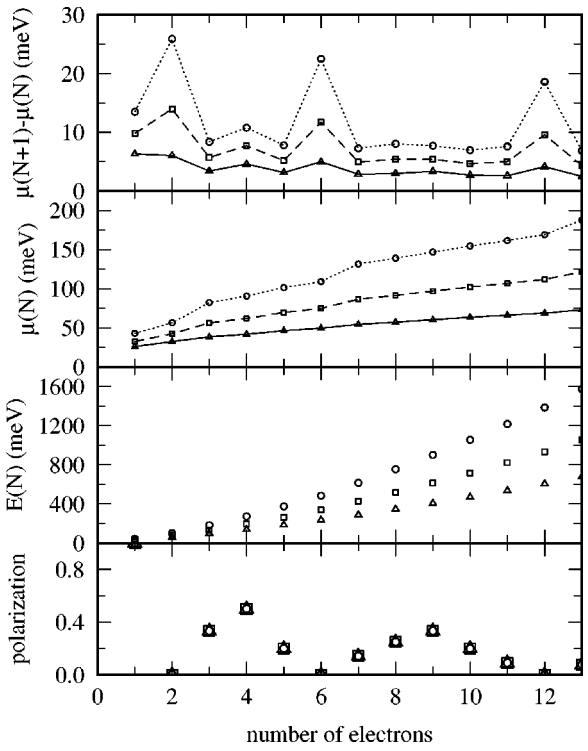

FIG. 1. Calculated properties of parabolic quantum dots as a function of the number of electrons N in the dot. The three confinement potentials are characterized by the harmonic confinements in meV units of $(\omega_x=\omega_y,\omega_z)=(20,45)$, (10,45), and (4,45), respectively. The symbols circles, boxes, and triangles represent the above quantum dots in descending order of x-y confinement strength of potentials. The capacitive energy $\mu(N+1)-\mu(N)$, chemical potential $\mu(N)$, and total energy $E(N)$ are shown in the top three panels. In the bottom panel is shown the spin polarization of the lowest-energy state defined as a ratio $(N^{\uparrow}-N^{\downarrow}/N^{\uparrow}+N^{\downarrow})$ of electrons with spins up $(N^{\uparrow})$ and down $(N^{\downarrow})$.

chemical potential calculations as shown in Eqs. (4) and (5). For the three values of $\omega_x(=\omega_y)$, the total energies increase monotonically with N. The chemical potential abruptly changes at $N=3$, $N=7$, and $N=13$ for the case of strong confinement of external potentials. The electron spins are fully unpolarized for $N=2$, 6, and 12, coinciding with the peaks of the capacitive energy of the quantum dot and a completely filled shell.

Our three-dimensional model quantum dot with strong confinement in the z direction has two-dimensional characteristics. This can be easily shown by the fact that the first excited state in the z direction is found at $N=13$ for the relative strong confinement of $\omega_z=45$ meV in the noninteracting electron picture. (However, we note that for the largest strength of the lateral confinement, $\omega_x=\omega_y=20$ meV, the energy of the third shell is near the lowest excitation energy for a state with a node in the z direction.) For the cylindrical symmetric two-dimensional quantum dot, the simple harmonic potential gives two nonnegative integer quantum numbers for the noninteracting single-particle energy spectrum, say, (n_x,n_y), and form a distinct energy group for each spin, $\{(0,0)\},\{(1,0),(0,1)\},\{(1,1),(2,0),(0,2)\},\ldots,$ and so on. These energy groups form a complete shell structure at $N=2$, 6, and 12 for the cylindrical two-dimensional quantum dot.

The chemical potential plotted vs N is approximately linear, the slope increasing when a new shell is occupied. We have found that the capacitive energies are peaked at the electron number $N=2$, 6, and 12 for each case of ω_x $(=\omega_y)=20$, 10, and 4 meV. These peak positions are in qualitative agreement with the experimental measurements addition energies of cylindrical quantum dots.[4] The calculated peak positions of the capacitive energy are consistent with results of the recent calculations[20] which used a two-dimensional exchange-correlation energy functional within the local-density approximation. The capacitive energies at $N=2$ and 6 are large compared to the noninteracting single-particle energy spacing ω_x of the quantum dot. The polarizations as a function of the number of electrons satisfy Hund's rule, i.e., there is maximum spin polarization for partially filled shells. In case of the relatively weak confinement of external potential $\omega_x=\omega_y=4$ meV, the capacitive energies at $N=2$, 6, and 12 are substantially suppressed, but still exhibit complete unpolarization due to shell filling. The effect is especially evident in the absence of a peak at $N=2$ when the confining potential is soft. The capacitive energies decrease as the shell index increases, which is consistent with experimental findings.[4] The capacitive energy is another version of the ionization energy minus electron affinity in density-functional theory as shown in Eq. (6). The calculated energy gaps of the three filled shells ($N=2$, 6, and 12) are in meV units (17.1, 15.0, 11.5), (7.8, 6.6, 5.3), and (2.6, 2.1, 1.8) for the three confinements of model quantum dots in descending order of x-y confinement strengths. The calculated energy gap is decreasing as the shell index increases from one to three for the three quantum dots considered here. This is mainly due to the electron-electron interactions in quantum dots. Thus, we confirmed that both the energy gap and capacitive energy decrease as a function of the shell index.

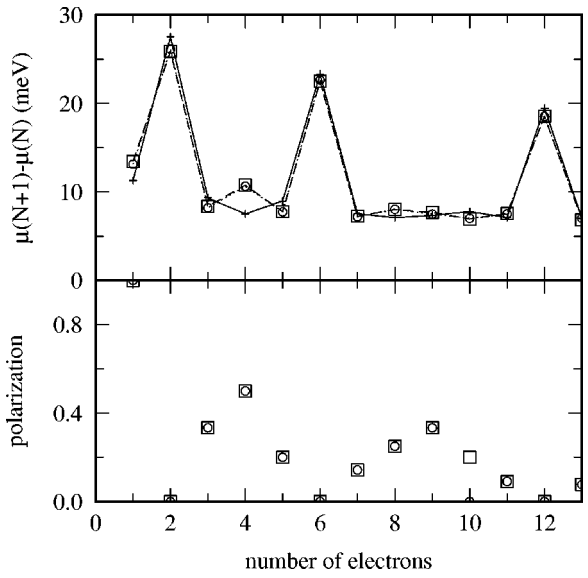

FIG. 2. The calculated capacitive energy $\mu(N+1)-\mu(N)$ and polarizations of the model quantum dot by GGA and LDA are compared. The circles represent the results of LDA, and the boxes represent the results of GGA. The crosses in capacitive energy plot represent the results from the spin-unpolarized version of the GGA calculations.

We compare the capacitive energies by LDA and GGA calculations in Fig. 2 and find no significant difference between two calculations with the different exchange-correlation energy per particle. In the LDA calculations, we find that the total energy of the spin configuration $(N^{\uparrow},N^{\downarrow})$ $=(5,5)$ is slightly lower (0.08 meV) than that of the spin configuration (6,4) at the electron number $N=10$; however, the energy difference is small compared to the numerical accuracy of our calculations. The spin-unpolarized calculation is generally acceptable for the capacitive energy calculations except at $N=4$, where the polarization has local maximum with respect to N in spin-polarized total-energy calculations, in contrast to the unpolarized calculation, which has a local minimum. The local maximum feature at $N=4$ is consistent with the experimental finding.[4] We also tested the Hartree approximation, completely neglecting the exchange-correlation effects, and found that it is not appropriate for the capacitive energy calculations. In the Hartree approximation, at the number of electrons $N=7$ and 10, we found negative capacitive energies; these unphysical results demonstrate the importance of the exchange-correlation effects. In the Hartree approximation the two-dimensional shell structure is not effectively stabilized, since there are only repulsive interactions between electrons, whereas the attractive exchange-correlation potential interaction for parallel spin stabilizes the completely filled shell electronic structures of quantum dot.

Within the density-functional theory the total energy can be decomposed into kinetic, external, Hartree, and exchange-correlation energies as shown in Eq. (3). In Fig. 3, we plot the kinetic and Hartree-exchange-correlation energies in units of the external potential energy to show the relative importance of their contributions to the total energy. We found that neither kinetic nor Hartree exchange correlation is greater than external potential energy for the three shells. As

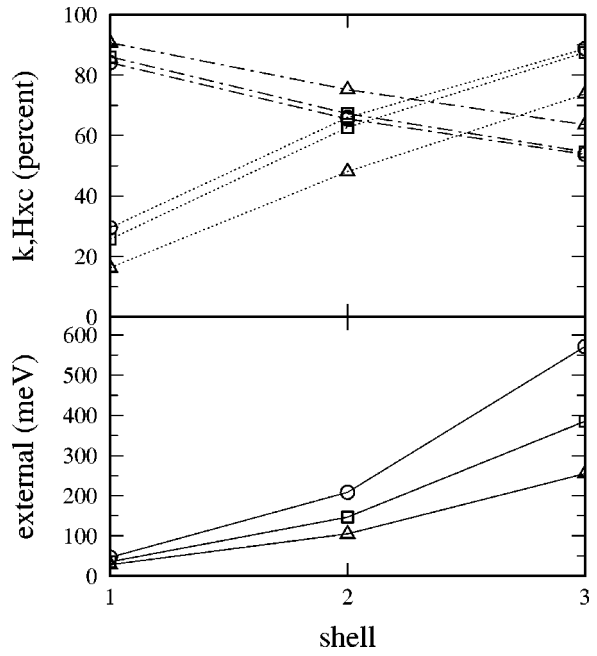

FIG. 3. The total-energy decomposition of the three-dimensional model quantum dots into the kinetic, external, and Hartree-exchange-correlation energies within the density-functional theory are shown. Due to the cylindrical symmetry of the confinement potentials, the first three shells are formed at $N=2$, 6, and 12. The external potential energies are shown in the lower panel and the relative magnitudes of the kinetic (k) and Hartree-exchange-correlation (Hxc) energy with respect to external potential energy are shown in the upper panel. The Hartree-exchange-correlation contribution is larger in the case of $N=12$ than the case of $N=2$. For the three cases of confinement potentials the same symbol notations are used as in Fig. 1.

shell index increases, the kinetic energy contribution decreases, while the Hartree exchange correlation increases. This shows that in the larger dot the electron-electron interaction is more important. As far as density-functional theory is concerned, the electronic structure is determined by the effective potential, which includes the external, Hartree, and exchange-correlation potentials. Therefore the shell-filling effects can be identified in the effective potentials. Nagaraja *et al.*[14] have found that the effective potential changes very little within a shell, but increases relatively more when a new shell is occupied.

The electron densities of the three filled shells for the confinement of $\omega_x=\omega_y=20$ and $\omega_z=45$ meV is shown in Fig. 4. We selected the x-y plane through the center of the confinement potentials. The electron density has a single maximum at the first filled shell. For the first filled shell ($N=2$), the electron-electron interaction is small compared to the kinetic and external potential energies, and the wave functions have no node so the density has a maximum at the center of dot. For the second filled shell ($N=6$), due to the single nodes in x and y direction the density has four maxima in x-y plane as shown in Fig. 4. In case of the third shell containing twelve electrons, due to the occupation of the states having two nodes density is again maximized at the center.

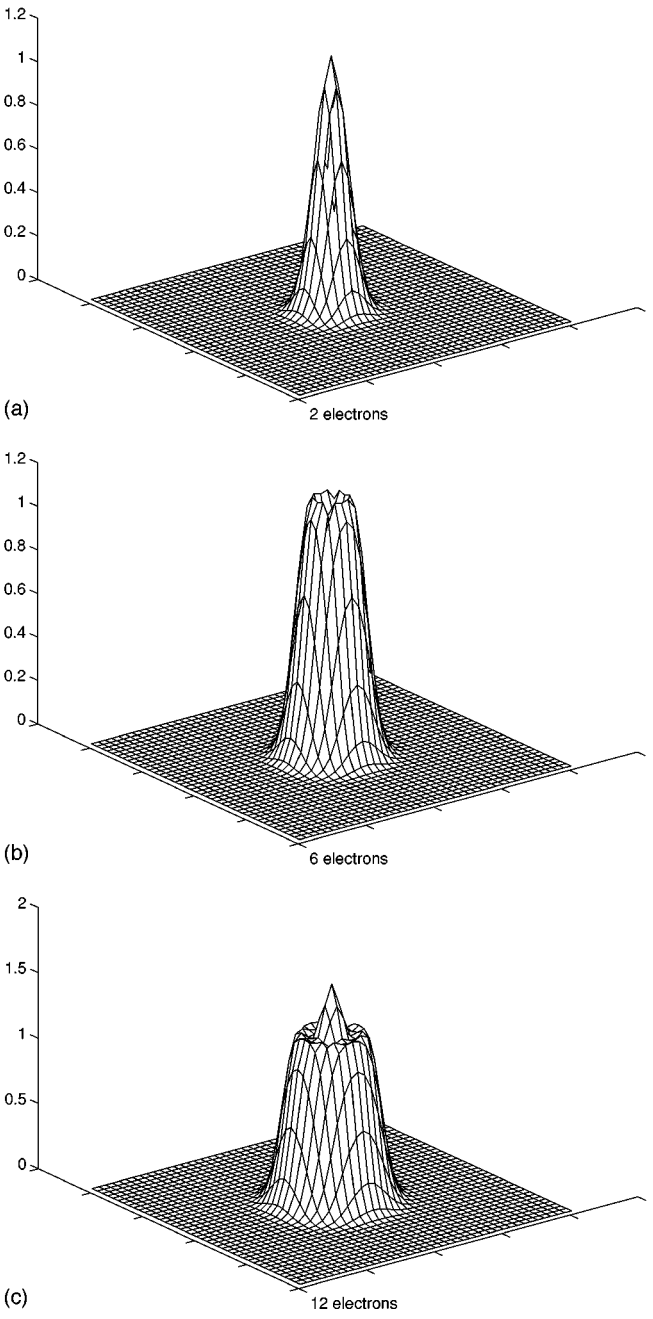

FIG. 4. The electron densities [in units of $1/(a_B^*)^3$] are shown in the x-y plane through the center the confinement potentials described by $(\omega_x=\omega_y,\omega_z)=(20,45)$ in units of meV.

B. Anisotropic confinement ($\omega_x\neq\omega_y$)

In order to see the effects of asymmetry of confinement potentials on the electronic structure we considered two different anisotropic confinement potentials in the x-y plane characterized by $(\omega_x,\omega_y)=(10,20)$ meV and $(\omega_x,\omega_y)=(7,10)$ meV for the fixed confinement of $\omega_z=45$ meV along the z direction. The latter case of confinement is closely related to the quad-gate planar quantum dot structures in experiment. The results including total energy, chemical potential, capacitive energy, and polarization are shown in Fig. 5. The relative peaks in the capacitive energy are not much higher than those of the cylindrical symmetric dot, partially due to the weakness of the confinement poten-

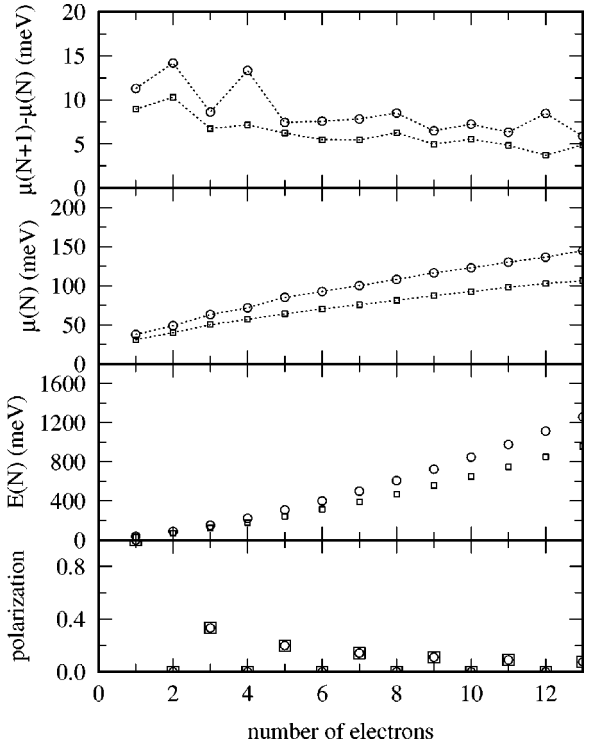

FIG. 5. The capacitive energies are calculated for the two anisotropic cases of confinements in meV units of $(\omega_x,\omega_y)=(10,20)$ and $(\omega_x,\omega_y)=(7,10)$. The circles and boxes represent the (10,20) and (7,10) confinement potentials.

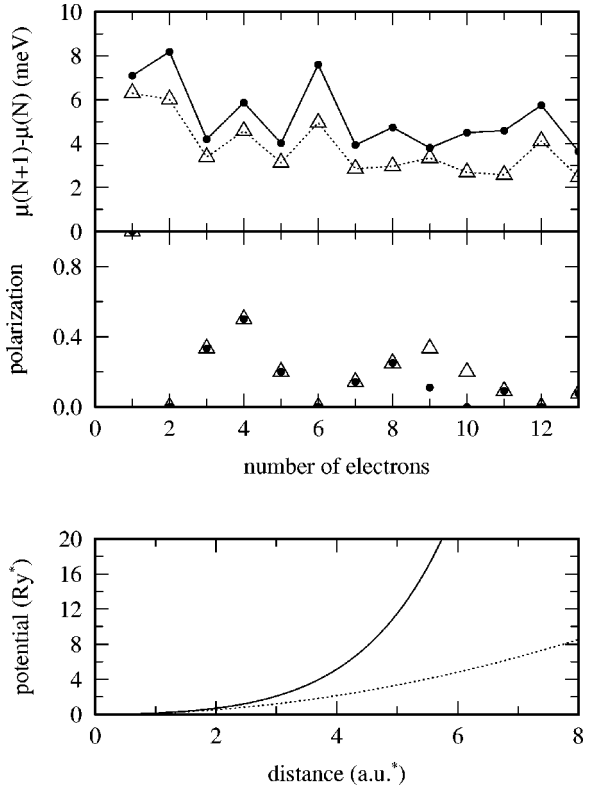

FIG. 6. The capacitive energies $\mu(N+1)-\mu(N)$, and polarizations for the two quantum dots are compared. The solid line represents the nonparabolic confinement potentials, while the dotted line represents the confinement of potential by $\omega_x=\omega_y=4$ meV.

tials. The capacitive energy peaks at $N=2$, 6, and 12 found for the symmetric confinement potential are not found for the anisotropic confinement potentials. Especially the peak in capacitive energy at $N=6$ is well suppressed. The polarization is zero for even numbers of electrons for both anisotropic cases of confinement potentials considered here. The second shell in anisotropic confinement potentials is formed at $N=4$ due to the symmetry breaking in x-y coordinate exchange. In these cases the spin-polarization effects are weaker than for the case of cylindrical symmetric confinement potentials. We can assign electronic states to the two-dimensional shell without considering interactions between electrons only for a small number of electrons in quantum dot $\{(0,0)\},\{(1,0)\},\{(0,1),(2,0)\},\{(1,1),(3,0)\},\ldots$ and so on, for the anisotropic x-y confinement of potential by $(\omega_x,\omega_y)=(10,20)$ meV. We can easily confirm the above shell structures of the anisotropic quantum dot from the peaks in the capacitive energy at $N=2$, 4, 8, and 12. In the case of anisotropic confining potential by $(\omega_x,\omega_y)=(10,20)$ meV, we found relatively small variations of the addition energy around $N=5$, 6, and 7 as shown in Fig. 5. This is basically a result of the filling procedures of the third shell characterized by nodes in wave functions $\{(0,1),(2,0)\}$ for each spin. To maximize the exchange interaction spin-parallel configuration is preferred during the filling of this shell. Nagaraja *et al.*[14] pointed out the existence of the ''Coulomb degeneracy,'' which is related to the lower addition energies in quad-gate dot for the charging of $N=5$, 6, and 7. This is consistent with our results even their calculations are based on the spin-unpolarized local-density approximation. Similar situation is also found in case of cylindrical symmetric potentials $(\omega_x=\omega_y)$ as shown in Fig. 1. For that case relatively small variations of the addition energy are found at $N=7$, 8, 9, 10, and 11 that correspond to the filling of the third shell.

C. Nonparabolic confinement potentials

We include the nonparabolic confinement potentials as shown in Eq. (8) to see the effects of the nonparabolicity in confinement,

$$V(\vec{r})=a_4(x^2+y^2)^2+a_6(x^2+y^2)^3+a_8(x^2+y^2)^4. \quad (8)$$

The coefficients are set to the values $a_4=5\times10^{-10}$ meV Å^{-4}, $a_6=5\times10^{-16}$ meV Å^{-6}, and $a_8=5\times10^{-22}$ meV Å^{-8}. This potential does not change the basic cylindrical symmetry of the two-dimensional parabolic potentials in Eq. (1). For the case of a small number of electrons and relatively strong lateral confinement potentials, the potential is still close to parabolic. The electronic structure of the large parabolic potentials of $\omega_x=\omega_y=20$ and $\omega_x=\omega_y=10$ meV with fixed $\omega_z=45$ meV is almost unchanged by the inclusion of the higher-order terms in the potential. However, for a weaker parabolic potential, $\omega_x=\omega_y=4$ meV, the nonparabolic terms in the potential change spin configurations at $N=9$ and 10. The total-energy differences between two spin configurations $\{(N^{\uparrow},N^{\downarrow})=(6,3)\rightarrow(5,4)\}$ and $\{(6,4)\rightarrow(5,5)\}$ are 0.39 and 0.55 meV for $N=9$ and 10, respectively. The node numbers (n_x,n_y) in wave function for x-y directions form a shell structure per spin such as $\{(0,0)\}$,

$\{(1,0),(0,1)\}$, $\{(2,0),(0,2)\}$, and $\{(1,1)\}$, . . . , and so on. We note that $\{(2,0),(0,2)\}$ and $\{(1,1)\}$ have the same energy in the pure harmonic confinement potential, while shell $\{(2,0),(0,2)\}$ has lower energy than that of the shell $\{(1,1)\}$ after inclusion of the nonparabolic potential. Consequently the filled shell structures are found at $N=2$, 6, 10, and 12. A similar energy splitting is found in more realistic square-gate dot electronic structure calculations by Nagaraja *et al.*[14] using the local-density approximation. In Fig. 6, we plot the capacitive energy, polarization, and the external potentials versus the distance from the center of dots. The solid line represents the external potential after inclusion of the nonparabolic part of the potential, while the dotted line represents the parabolic confinement of potential by $\omega_x=\omega_y=4$ meV. The nonparabolic terms in the confinement potential increase the capacitive energy relative to the case of the pure parabolic potential since the nonparabolic terms cause greater confinement. In the weak parabolic confinement case here $\omega_x=\omega_y=4$ meV, the capacitive energy at $N=2$ does not form a peak as shown in Fig. 6. However, the capacitive energy peak at $N=2$ for the nonparabolic confinement is well established after inclusion of the nonparabolic confinement potentials. The calculated gaps for the first three shells are increased in meV units from (2.6, 2.1, 1.8) to (3.7, 3.6, 2.2) after inclusion of the nonparabolic potentials. This is also consistent with the overall increment in the capacitive energy.

IV. CONCLUSIONS

The electronic structure of the anisotropic parabolic and nonparabolic quantum dots have been investigated with three-dimensional confinement potentials using density functional theory within the framework of the generalized-gradient approximation. By performing three-dimensional electronic structure calculations, we confirmed that the shell structures of quantum dots very strongly confined in the z direction have two-dimensional character. Using a Laplacian operator discretized on uniform grids with a high-order finite difference method, the Poisson equation and spin-polarized Kohn-Sham equations were solved iteratively with the efficient preconditioned conjugate gradient relaxation techniques. The quantization effects due to the confinement, spin polarization, and exchange-correlation were compared. We found that in the larger quantum dot the electron-electron interaction is more important than the effect due to quantum confinement. The capacitive energy for fillings of up to thirteen electrons was obtained by self-consistent total-energy calculations. The calculated energy gap in the eigenvalue spectrum and the capacitive energy are a decreasing function of the shell index, and the peak positions of the capacitive energy at the number of electrons $N=2$, 6, and 12 for the cylindrical symmetric quantum dot are in good agreement with experimental data.

ACKNOWLEDGMENTS

This work was supported by a CRI grant of the University of Illinois. V.R., J.P.L., and R.M.M. acknowledge, respectively, support by GRT, and NSF Grant No. ECS 96-12780 and No. DMR94-22496.

[1] M. A. Kastner, Phys. Today **46** (1), 24 (1993).
[2] R. C. Ashoori, H. L. Stormer, J. S. Weiner, L. N. Pfeiffer, R. W. Baldwin, and K. W. West, Phys. Rev. Lett. **71**, 613 (1993).
[3] J. Weis, R. J. Haug, K. v. Klitzing, and K. Ploog, Phys. Rev. Lett. **71**, 4019 (1993).
[4] S. Tarucha, D. G. Austing, T. Honda, R. J. van der Hage, and L. P. Kouwenhoven, Phys. Rev. Lett. **77**, 3613 (1996).
[5] A. Lorke, J. P. Kotthaus, and K. Ploog, Phys. Rev. Lett. **64**, 2559 (1990).
[6] T. Demel, D. Heitmann, P. Grambow, and K. Ploog, Phys. Rev. Lett. **64**, 788 (1990).
[7] C. T. Liu, K. Nakamura, D. C. Tsui, K. Ismail, D. A. Antoniadis, and H. I. Smith, Appl. Phys. Lett. **55**, 168 (1989).
[8] W. Hansen, T. P. Smith, III, K. Y. Lee, J. A. Brum, C. M. Knoedler, J. M. Hong, and D. P. Kern, Phys. Rev. Lett. **62**, 2168 (1989).
[9] G. W. Bryant, Phys. Rev. Lett. **59**, 1140 (1987).
[10] P. A. Maksym and T. Chakraborty, Phys. Rev. Lett. **65**, 108 (1990); Phys. Rev. B **45**, 1947 (1992).
[11] J. J. Palacios, L. Martin-Moreno, G. Chiappe, E. Louis, and C. Tejedor, Phys. Rev. B **50**, 5760 (1994).
[12] A. Kumar, S. E. Laux, and F. Stern, Phys. Rev. B **42**, 5166 (1990).
[13] D. Jovanovic and J.-P. Leburton, Phys. Rev. B **49**, 7474 (1994).
[14] S. Nagaraja, P. Matagne, V.-Y. Thean, J.-P. Leburton, Y.-H. Kim, and R. M. Martin, Phys. Rev. B **56**, 15 752 (1997).
[15] M. Stopa, Y. Aoyagi, and T. Sugano, Surf. Sci. **305**, 571 (1994); M. Stopa, Phys. Rev. B **54**, 13 767 (1996).
[16] N. F. Johnson and M. C. Payne, Phys. Rev. B **45**, 3819 (1992).
[17] M. Macucci, K. Hess, and G. J. Iafrate, J. Appl. Phys. **77**, 3267 (1995).
[18] G. J. Iafrate, K. Hess, J. B. Krieger, and M. Macucci, Phys. Rev. B **52**, 10 737 (1995).
[19] M. Fujito, A. Natori, and H. Yasunaga, Phys. Rev. B **53**, 9952 (1996).
[20] M. Macucci, K. Hess, and G. J. Iafrate, Phys. Rev. B **55**, R4879 (1997).
[21] M. Koskinen, M. Manninen, and S. M. Reimann, Phys. Rev. Lett. **79**, 1389 (1997).
[22] J. R. Chelikowsky, N. Troullier, and Y. Saad, Phys. Rev. Lett. **72**, 1240 (1994); J. R. Chelikowsky, N. Troullier, K. Wu, and Y. Saad, Phys. Rev. B **50**, 11 355 (1994).
[23] B. Fornberg and D. Sloan, in *Acta Numerica 1994*, edited by A. Iserles (Cambridge University Press, Cambridge, 1994), pp. 203–267.
[24] P. Hohenberg and W. Kohn, Phys. Rev. **136**, 864B (1964); W. Kohn and L. J. Sham, *ibid.* **140**, 1133A (1965).
[25] R. O. Jones and O. Gunnarsson, Rev. Mod. Phys. **61**, 689 (1989).

[26] J. P. Perdew, K. Burke, and M. Ernzerhof, Phys. Rev. Lett. **77**, 3865 (1996); I.-H. Lee and R. M. Martin, Phys. Rev. B **56**, 7197 (1997).

[27] D. M. Ceperley and B. J. Alder, Phys. Rev. Lett. **45**, 566 (1980); J. Perdew and A. Zunger, Phys. Rev. B **23**, 5048 (1981).

[28] M. C. Payne, M. P. Teter, D. C. Allan, T. A. Arias, and J. D. Joannopoulos, Rev. Mod. Phys. **64**, 1045 (1992).

[29] D. M. Bylander, L. Kleinman, and S. Lee, Phys. Rev. B **42**, 1394 (1990).

[30] T. Hoshi, M. Arai, and T. Fujiwara, Phys. Rev. B **52**, R5459 (1995).

[31] A. P. Seitsonen, M. M. Puska, and R. M. Nieminen, Phys. Rev. B **51**, 14 057 (1995); M. P. Teter, M. C. Payne, and D. C. Allan, *ibid.* **40**, 12 255 (1989).

[32] P. Pulay, Chem. Phys. Lett. **73**, 393 (1980).